Synaptic vesicles dynamics in neocortical epilepsy

Eleonora Vannini[1,2,3,*,#], Laura Restani[1], Marialaura Dilillo[4], Liam McDonnell[4], Matteo Caleo[1,5,#], Vincenzo Marra[2,*]

[1] Neuroscience Institute, National Research Council (CNR), via G. Moruzzi 1, 56124 Pisa, Italy

[2] Department of Neuroscience, Psychology and Behaviour, University of Leicester, Leicester LE1 7RH, United Kingdom

[3] Fondazione Umberto Veronesi, Piazza Velasca 5, 20122 Milan, Italy

[4] Fondazione Pisana per la Scienza Onlus (FPS), via Ferruccio Giovannini 13, San Giuliano Terme, 56017 Pisa, Italy

[5] Department of Biomedical Sciences, University of Padua, via G. Colombo 3, 35121 Padua, Italy

Running Title: Synaptic vesicles dynamics in neocortical epilepsy

Keywords: epilepsy; synaptic vesicles; hyperexcitability; visual cortex; visual processing; tetanus neurotoxin

*Corresponding authors: Dr Eleonora Vannini, Email e.vannini@in.cnr.it; Dr Vincenzo Marra, Email vm120@le.ac.uk

[#]Equal contribution as senior authors

Abstract

Neuronal hyperexcitability often results from an unbalance between excitatory and inhibitory neurotransmission, but the synaptic alterations leading to enhanced seizure propensity are only partly understood. Taking advantage of a mouse model of neocortical epilepsy, we used a combination of photoconversion and electron microscopy to assess changes in synaptic vesicles pools *in vivo*. Our analyses reveal that epileptic networks show an early onset lengthening of active zones at inhibitory synapses, together with a delayed spatial reorganization of recycled vesicles at excitatory synapses. Proteomics of synaptic content indicate that specific proteins were increased in epileptic mice. Altogether, our data reveal a complex landscape of nanoscale changes affecting the epileptic synaptic release machinery. In particular, our findings show that an altered positioning of release-competent vesicles represent a novel signature of epileptic networks.

Introduction

Epilepsy is a disorder of the central nervous system that affects around 50 million people worldwide and it is characterized by recurrent spontaneous seizures, that are the clinical manifestation of an excessive hypersynchronous discharge of a population of neurons (Bromfield and Cavazos, 2006). Despite all the available treatments, one third of patient develop a drug-resistant form of epilepsy (Kwan et al.; Sharma et al., 2015). The propensity to develop seizures is due to brain damage, in lesional epilepsy (Pitkänen and Immonen, 2014; Wasilewski et al., 2020; Wie Børsheim et al., 2020), or to an altered synaptic function at excitatory and/or inhibitory terminals, in non-lesional epilepsy (Wykes et al., 2012; Farisello et al., 2013; Corradini et al., 2014; Ferecskó et al., 2015; Snowball et al., 2019). Specifically, chronic epilepsy is thought to result from a synaptic reorganization that leaves permanent marks on cortical networks and may lead to network dysfunction, cognitive deficits and impaired information processing (Pitkänen et al., 2013, 2015; Holmes, 2015; Vannini et al., 2016). Epileptic networks display several modifications in synaptic function and structure at the level of presynaptic boutons, post-synaptic structures and the glial processes enwrapping them (Bernard, 2010). In the presynaptic compartment, recent technological advances have allowed a detailed characterization of the size and spatial organization of functional vesicle pools. These parameters correlate with

measures of synaptic strength and are altered following plasticity-inducing stimuli (Rey et al., 2020). However, such ultrastructural readouts of synaptic function have not been applied thus far to the study of epileptogenic modifications or their consequences.

The correct functioning of neuronal networks requires precise modulation of excitatory and inhibitory activity (Xue et al., 2014; Rossi et al., 2017; Rubin et al., 2017; Sohal and Rubenstein, 2019). When network activity is tipped out of balance, a number of cellular processes take place to re-establish its normal function (Turrigiano, 2012). The processes underlying homeostatic plasticity can affect cellular activity and synaptic output (Wefelmeyer et al., 2016). Following a perturbation, neurons attempt to restore their baseline firing rates and dynamic range by regulating their intrinsic excitability, probability of neurotransmitter release and neurotransmitter receptor expression (Davis and Müller, 2015). Central synapses have the ability to plastically adapt to new conditions by dynamically scaling up and down their output. Such regulation has been demonstrated to occur during development, sleep and learning. However, much less is known about the mechanisms of homeostatic scaling as a consequence of a pathological, system-level perturbation *in vivo* (Turrigiano, 2008, 2012; González et al., 2019).

Here we took advantage of a well-characterised model of chronic, focal epilepsy in the visual cortex (Mainardi et al., 2012; Chang et al., 2018) to investigate synaptic changes in hyperexcitable networks. Tetanus neurotoxin (TeNT) is a metalloprotease that cleaves the synaptic protein VAMP/synaptobrevin leading to the establishment of a focal cortical hyperexcitability, with electrographic seizures that persist for several weeks after TeNT wash out (Nilsen et al., 2005; Jiruska et al., 2010; Mainardi et al., 2012; Vannini et al., 2016; Snowball et al., 2019). Despite many studies characterizing TeNT-induced epilepsy (i.e. seizures manifestation), very little is known about the persistent synaptic changes that underpin chronic, spontaneous seizures. The absence of neuronal loss and gliosis, together with the persistence of spontaneous seizures, chronically altered neural processing and structural modifications of both dendritic spines and branches suggest that synaptic modifications occur and last after TeNT clearance (Mainardi et al., 2012; Vannini et al., 2016). Here, using FM1-43FX and activity-dependent labelling of synaptic vesicles, we simultaneously investigated function and ultrastructure of both excitatory and inhibitory terminals, in acute and chronic phases of TeNT-induced epilepsy. We combined this approach with an unbiased measure of proteins content in the two phases of hyperexcitability, isolating synaptosomes at different time points after TeNT injection, and assessing by electrophysiological recordings the impact of inhibiting Carboxypeptidase E (CPE), upregulated in epileptic mice, on seizures occurrence.

Methods

Animals and TeNT injections

Adult (age > postnatal day 60) C57BL/6J mice used in this study were reared in a 12h light-dark cycle, with food and water available *ad libitum*. All experimental procedures were conducted in conformity with the European Communities Council Directive *n*◦ 86/609/EEC and were approved by the Italian Ministry of Health. TeNT (Lubio; Lucerne, Switzerland; 0.1—0.2 ng) or RSA (Rat Serum Albumin) solutions in PBS were intracranially injected into the primary visual cortex (i.e. 0.0 mm anteroposterior, 2.7 mm lateral to the lambda suture and at a cortical depth of 0.65 mm) ; of anesthetised (ketamin/Xylazine 100-10 mg/Kg) mice. After surgery, a glucose solution (5 % in saline) was subcutaneously administered and recovery of animals was carefully monitored. Paracetamol was added in drinking

77 water for 3 days. Additional details can be found in Mainardi et al., 2012; Vallone et al., 2016; Vannini et al., 2016,
78 2017. No behavioural seizures are detectable in those animals, as already reported in (Mainardi et al., 2012; Vannini et
79 al., 2016).

80 FM 1-43FX injection and visual stimulation

81 Control and epileptic mice, deeply anesthetized with urethane (7 ml/kg; 20 % solution in saline, i.p.; Sigma)
82 and placed in a stereotaxic apparatus, received an injection of FM 1-43FX dye into the primary visual cortex, layers II-
83 III (i.e. 0.0 mm anteroposterior and 2.7 mm lateral to the lambda suture, 0.7 mm depth). FM1-43FX is a non-
84 permeable styryl dye that labels the cell membrane. Once synaptic vesicles fuse with the cell membrane, molecules of
85 FM1-43FX diffuses laterally along the membrane previously comprising the vesicle. As vesicles undergo endocytosis,
86 as part of their recycling, the dye is trapped inside the recently released vesicles (Marra et al., 2014). 3 min later,
87 animals were stimulated for 10 min with square-wave gratings (1 Hz, 0.06 c/deg, contrast 90%) and flashes of light. All
88 visual stimuli were computer-generated on a display (Sony; 40 x 30 cm; mean luminance 15 cd/m2) by a VSG card
89 (Cambridge Research Systems). Mice, still under anaesthesia, were kept in the dark and perfused through the heart
90 with a fresh solution of 6% glutaraldehyde, 2% formaldehyde in PBS, as described in (Jensen and Harris, 1989) right
91 after the end of the visual stimulation
92

93 Photoconversion and Electron Microscopy analysis

94 All the following procedures were made in the dark. The protocol followed is described in detail in (Marra et
95 al., 2014). Briefly, embedded in EPON, slices were collected with an ultramicrotome serial sections (70 nm thickness)
96 and placed in grids at RT. Thereafter, sections could be viewed with a transmission electron microscope fitted with a
97 cooled CCD camera. Images were acquired using local landmarks to identify the same target synapse in consecutive
98 sections and analysed using Image J/Fiji (NIH) and a custom script in Python (Python.org). At ultrastructural level,
99 target synapses (visual cortex, layers II-III) were randomly chosen and synaptic vesicles were scored based on their
100 vesicle luminal intensity using methods outlined previously (Darcy et al., 2006), image names were changed to ensure
101 that the experimenters were blind to the experimental condition of each electron micrograph. A terminal was
102 considered inhibitory if no spine or postsynaptic density could be observed in the middle section and in at least one of
103 the adjacent sections. As expected (Meyer et al., 2011; Tremblay et al., 2016; van Versendaal and Levelt, 2016; Lim et
104 al., 2018), inhibitory terminals were estimated to be 15-25% of the total.
105

106 Synaptosomes extraction and proteomic analysis

107 Synaptosomes were extracted using a slightly modified protocol taken from (Giordano et al., 2018). Visual
108 cortices were gently homogenized in 500 μl of ice cold homogenizing buffer (0.32 M sucrose, 1 mM EDTA, 1mg/ml
109 BSA, 5 mM HEPES pH 7.4, proteases inhibitors) and centrifuged 10 min at 3000 g at 4°C; supernatant was recovered
110 and centrifuged again for 15 min at 14000 g at 4°C. After discarding supernatant, the pelleted synaptosomes were
111 suspended in 110 μl of Krebs-Ringer Buffer and 90 μl of Percoll (Sigma-Aldrich) were added. A 2 min spin (14000 rpm,
112 4°C) was performed and enriched synaptosomes were recovered from the surface of the solution with a P1000 tip and
113 resuspended in 1ml of Krebs-Ringer buffer. After an additional spin of 2 min (14000 rpm, 4°C), the supernatant was
114 discarded and the pellet resuspended in 20 μl of RIPA buffer.

115

116 Proteomics sample preparation and data analysis

117 Trypsin/LysC mix Mass Spec grade was purchased from Promega (Madison, WI). Tandem Mass Tags (TMT 10-
118 plex) kits and microBCA protein assay kit were purchased from Thermo Fisher Scientific (Rockford, IL). All other
119 reagents and solvents were purchased from Sigma-Aldrich (St. Louis, MO). Synaptosomes proteome extracts were
120 quantified with a micro BCA protein assay and aliquots of 3.5 µg of proteins were diluted to 40 µL of
121 RIPA/Trifluoroethanol (TFE) 50/50. Paramagnetic beads were added to each sample and further processed following a
122 modified SP3 protocol for ultrasensitive proteomics as previously described (Pellegrini et al., 2019). Synaptosomes
123 proteins were reduced alkylated and digested with a mixture of trypsin/Lys-C (1:20 enzyme to protein ratio). Digested
124 peptides were then quantified, and labelled with TMT 10-plex: samples were block randomized
125 (www.sealedenvelope.com) over 5 TMT sets. Each TMT set included 2 normalization channels for batch corrections
126 built pooling an aliquot from each digested synaptosome sample (Plubell et al., 2017). TMT sets underwent high pH
127 fractionation on an AssayMap Bravo (Agilent technologies) and fractions run on a nano-LC (Easy1000 Thermo Fisher
128 Scientific) equipped with a 50 cm EasySpray column and coupled with an Orbitrap Fusion for MS3 analysis (Thermo
129 Fisher Scientific). Experimental details regarding sample fractionation and LC-MS/MS runs have been already reported
130 elsewere (Pellegrini et al., 2019). Data were analysed using Proteome Discoverer 2.1. TMT data were normalized by
131 internal reference scaling (Plubell et al., 2017).

132

133 Electrophysiological recordings and drugs administration

134 Surgery was performed as described in (Spalletti et al., 2017), but the small craniotomy was centred at 3 mm
135 lateral to Lambda and performed in TeNT/RSA-injected hemisphere. Neuronal activity was recorded with a
136 NeuroNexus Technologies 16-channel silicon probe with a single-shank (A1x16-3mm-50-177) mounted on a three-axis
137 motorized micromanipulator and slowly lowered into the portion of visual cortex previously injected with TeNT or RSA
138 solution. The tip of the probe was positioned at the depth of 1 mm so that the electrode contacts (spaced by 50
139 microns) sampled activity from all cortical layers. Before the beginning of the recording, the electrode was allowed to
140 settle for about 10 min. Local Field Potentials (LFP) signals were acquired at 1 kHz and bandpass filtered (0.3 Hz to 200
141 Hz) with a 16-channel Omniplex recording system (Plexon, Dallas, TX). Local Field Potentials (LFP) were computed
142 online and referred to the ground electrode in the cerebellum. In order to verify whether interacting with
143 Carboxypeptidase E (CPE) would change epileptic activity, we topically applied over the craniotomy 2 µL of PBS
144 containing 25 µM of 2- guanidinoethylmercaptosuccinic acid (GEMSA; Sigma-Aldrich) without removing the electrode.
145 Neural signals were acquired at regular time intervals up to 30 min after GEMSA delivery to verify the effect and the
146 penetration of the drug in the cortical layers. At the end of the experiment animals were sacrificed. Data were
147 analysed offline with NeuroExplorer software (Plexon Inc, USA) and with custom made Python interfaces (Python.org).
148 Movement artifacts were removed offline. The coastline analysis was calculated as the sum of the absolute difference
149 between successive points (Wykes et al., 2012).

150

151 Statistical analysis

Statistical analysis was performed with Graph Pad (version 8) except for proteomics analysis, in which we used Perseus. Normality of distributions was assessed with D'Agostino test and appropriate test was chosen accordingly.

Results

Ultrastructural investigation of synaptic vesicle function in hyperexcitable networks

Our studies included three groups of C57BL/6 mice with injections into the primary visual cortex (V1): a control group injected with vehicle (Control), an Acute epileptic group tested 10 days after TeNT injection in V1 and a Chronic epileptic group tested 45 days after TeNT injection in V1. Synaptic vesicles from 3 animals in each of these groups were labelled by infusing FM1-43FX in the visual cortex while presenting a series of visual stimuli (**Fig. 1A**). After fixation, photoconversion and processing for electron microscopy, we were able to label individual vesicles at excitatory (asymmetrical) and inhibitory (symmetrical) synapses (**Fig. 1A**). This approach allowed us to identify individual synaptic vesicles, released and recycled in the presence of FM1-43FX, as having an electron dense lumen, while non-released vesicles present a clear lumen and a darker membrane (Marra et al., 2012). First, we investigated the length of the active zone as a readout of synaptic activity independent of our labelling protocol (Harris and Weinberg, 2012). Surprisingly, we found an increase in the length of inhibitory synapses' active zone in the acute phase (**Fig. 1B**), normally associated with increased release. However, the released fraction of inhibitory vesicles (number of released vesicles over total number of vesicles) is reduced in animals injected with TeNT (**Fig. 1C**), shown to preferentially impair inhibitory release (Schiavo et al., 2000). No differences in active zone length and released fraction of vesicles were found at excitatory synapses (**Fig. 1B, 1C**). Interestingly, the total number of vesicles across control and epileptic groups does not change significantly neither at excitatory (Control: mean= 52.16, SD=35.47, n= 49; Acute: mean= 56.23, SD=29.81, n=59; Chronic: mean= 51.28, SD=19.39, n= 124; data not shown) nor inhibitory synapses (Control: mean= 40.76, SD=14.38, n=17; Acute: mean= 54.33, SD=36.12, n=18; Chronic: mean= 54.33, SD=19.91, n=30; data not shown).

FIGURE 1

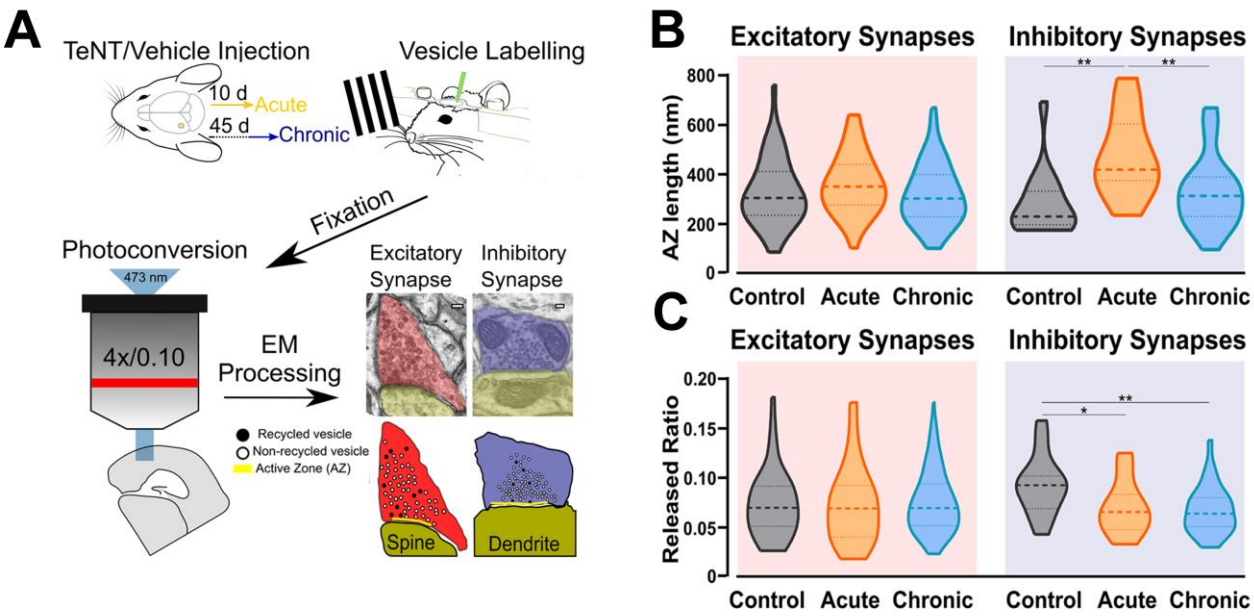

Figure 1: *Ultrastructural and functional changes at presynaptic terminals of TeNT-injected mice.* ***A****) Diagrammatic representation of labelling protocol. Visual cortices from mice in Control, Acute and Chronic groups were infused with FM1-43FX during mild visual stimulation. Brains were rapidly fixed and sliced to allow photoconversion of FM1-43FX signal before processing for electron microscopy. Individual presynaptic terminals were classified as excitatory (asymmetrical synapses, red) or inhibitory (symmetrical synapses, blue); size, position and numbers of active zone (AZ, yellow), non-released vesicles (open circles) and released vesicles (black circles) were analysed (scale bars 100 nm).* ***B****) Left: Active zone (AZ) length in Control (grey), Acute (orange) and Chronic (blue) epileptic mice at excitatory synapses; no differences between the groups (Kruskal-Wallis test, p = 0.10). Distribution, median and quartiles shown for each group; Control n=41; Acute n=46; Chronic n=118. Right: Active zone (AZ) length in Control (grey), Acute (orange) and Chronic (blue) epileptic mice at inhibitory synapses (Kruskal-Wallis test, p < 0.01, Control vs Acute p<0.01, Control vs Chronic p>0.05, Chronic vs Acute p<0.01). Distribution, median and quartiles shown for each group; Control n=15; Acute n=14; Chronic n=29.* ***C)*** *Left: Released fraction of synaptic vesicles (labelled vesicles/total vesicles) in Control (grey), Acute (orange) and Chronic (blue) epileptic mice at excitatory synapses; no differences between the groups (Kruskal-Wallis test, p = 0.67). Distribution, median and quartiles shown for each group; Control n=47; Acute n=57; Chronic n=118. Right: Released fraction of synaptic vesicles of Control (grey), Acute (orange) and Chronic (blue) epileptic mice at inhibitory synapses. (Kruskal-Wallis test, p < 0.05, Control vs Acute p<0.05, Control vs Chronic p<0.01, Chronic vs Acute p>0.05). Distribution, median and quartiles shown for each group; Control n=16; Acute n=16; Chronic n=30.*

Changes in docking and positioning of activated vesicles at excitatory synapses in chronic epilepsy

After quantifying direct and indirect measures of vesicular release, we examined the spatial distribution of released and non-released vesicles within presynaptic terminals. We started by analysing the released fraction in the docked and non-docked populations of vesicles. As described before for excitatory synapses (Marra et al., 2012), the Control group showed a higher released fraction in the docked population, similar results were found in the Acute group. Conversely, in the Chronic group the released fraction was higher in the non-docked population at excitatory synapses (**Fig. 2A**). We also report that inhibitory synapses have a higher released fraction in the docked population, which does not seem to be affected by the induction of epilepsy (**Fig. 2A**). To gain insight on the effect observed at excitatory synapses of the Chronic group, we compared the distance of released and non-released vesicles from the active zone (**Fig. 2B**). We reasoned that if the effect is specific to the ability of released vesicles to dock, their position

within the terminal should not be affected. We examined the cumulative fraction of the distance of released and non-released vesicles from their closest point on the active zone. At excitatory synapses, in Control and Acute groups the released vesicle population are closer to the active zone compared to the non-released population. However, in the Chronic group released excitatory vesicles do not show a spatial bias towards the active zone, that was instead observed in the other groups (**Fig. 2B**). At inhibitory synapses, the distances of vesicular populations to the active zone has a different pattern, with no difference between released and non-released population in Control and Acute groups and with a spatial bias of released vesicles towards the active zone in the Chronic group (**Fig. 2B**). As a visual representation of the distribution of released vesicles at excitatory and inhibitory across the three conditions, we generated 2D histograms of the distribution of released vesicles within spatially normalised terminals, with the centre of the active zone at the origin of the X axis (**Fig. 2C**). This representation shows a clear broadening of the distribution of released excitatory vesicles in the chronic phase.

FIGURE 2

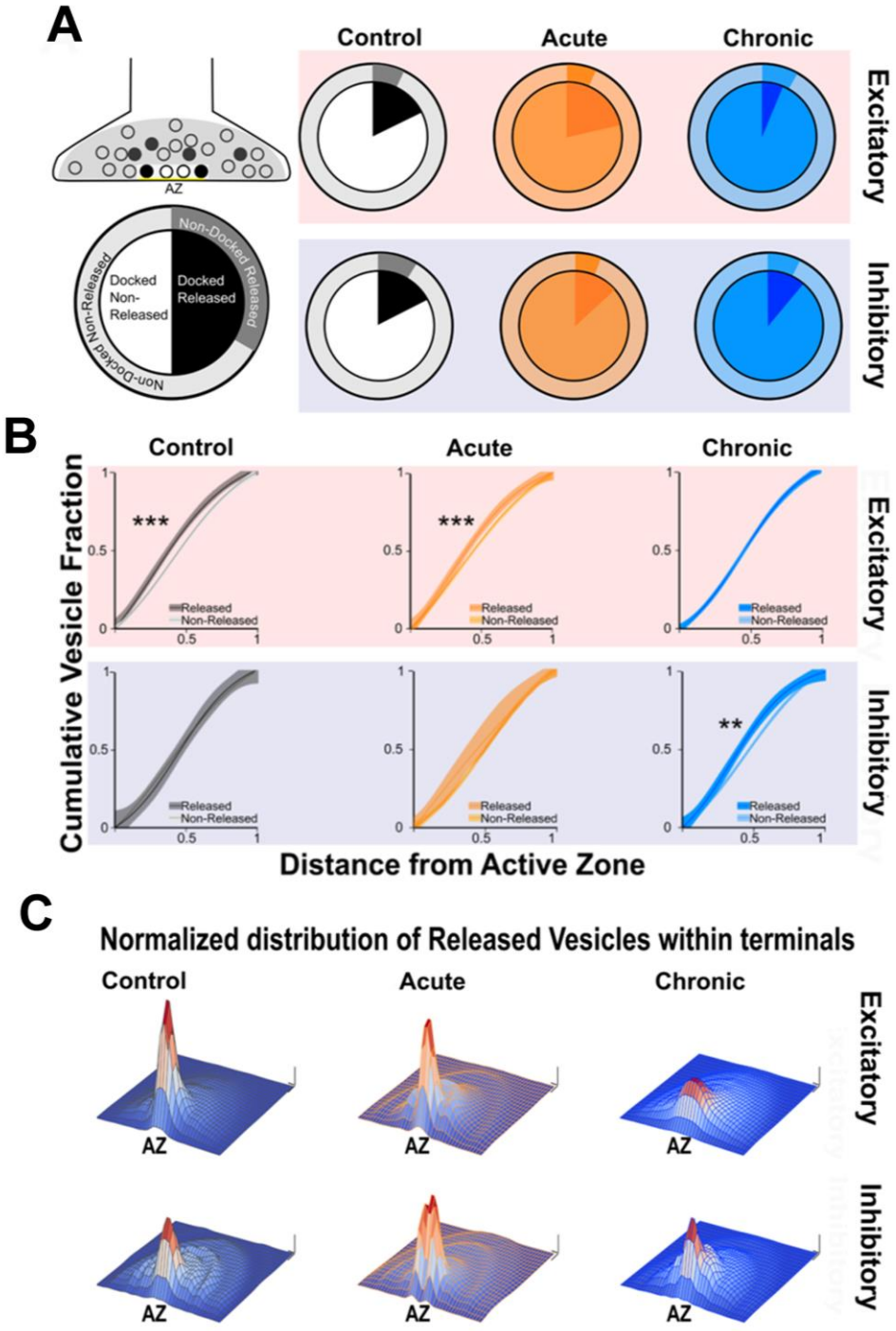

199

Figure 2**: Changes in released vesicles' docking and spatial organization in chronic phase of epilepsy.* ***A*) Ratio of released vesicles in the docked and undocked population. Left: Diagram and legend for each pie chart. Top: Excitatory synapses' ratio of released vesicles (darker) in docked (inner pie chart) and undocked population (outer pie chart) in Control (grey), Acute (orange) and Chronic (blue) groups. Only the Chronic group shows a significant difference from expected frequencies based on control observation (Chi-squared test: p< 0.001). Bottom: Inhibitory synapses' ratio of released vesicles (darker) in docked (inner pie chart) and undocked population (outer pie chart) in control (grey), acute (orange) and chronic (blue) groups.* ***B****) Distance of released or non-released vesicles to the closest point on the active zone. Left: Diagram representing of how distance measures were taken at each synapse.*

Top: Sigmoid fit and 95% confidence interval of cumulative fraction of distance between released and not-released synaptic vesicles to the active zone at excitatory synapses in Control (grey), Acute (orange) and Chronic (blue) epileptic mice. Bottom: Sigmoid fit and 95% confidence interval of cumulative fraction of distance between released and not-released synaptic vesicles to the active zone at inhibitory synapses in Control (grey), Acute (orange) and Chronic (blue) epileptic mice. Paired t-test, Excitatory synapses: Control mice p = 0.0002 (n=40), Acute mice p = 0.0006 (n=41), Chronic mice p = 0.298 (n=112). Paired t-test, Inhibitory synapses: Control mice p = 0.06 (n=14), Acute mice p = 0.135 (n=13), Chronic mice p = 0.001 (n=28). ***C****) 2D histograms of released vesicles distribution at excitatory (top) and inhibitory (bottom) synapses across the three conditions with active zone at the origin of the XY plane. Control (grey), Acute (orange) and Chronic (blue). Each synapse was spatially normalised (X and Y axes) and frequency is plotted on the Z axis. Scale bars: 0.1 normalised size X and Y; 0.1 fraction Z axis.*

200

201 Upregulation of synaptic proteins involved in vesicle positioning in Acute and Chronic epilepsy phases

202 To better understand molecular changes taking place in epileptic synapses, we performed an in-depth
203 proteomic analysis of visual cortex synaptosomes. The expression profile of 1991 synaptic proteins extracted from
204 animals in the acute and chronic phase of epilepsy was compared with controls. Using a fold change cut-off of 0.6, we
205 found a total of 70 regulated proteins (51 proteins upregulated and 19 downregulated; **Fig. 3A, 3B**). As expected
206 following TeNT injection, the Acute group showed a significant downregulation of VAMP1 and VAMP2 (Mainardi et al.,
207 2012; Vannini et al., 2016). Interestingly, a few synaptic proteins remained upregulated at both stages of epilepsy,
208 suggesting that one single TeNT injection is sufficient to induce persistent plastic changes. Proteins involved in
209 synthesis of regulatory peptides, WNT pathway, immune response and membrane-trafficking were upregulated in
210 hyperexcitable mice (i.e. Dickhopf related protein 3, Complement component 1q, Synaptotagmin 5, Semaphorin 4a,
211 Carboxypeptidase E - CPE, Chromogranin B). The upregulation of neuropeptides was in line with previous reports
212 (Vezzani and Sperk, 2004; Kovac and Walker, 2013; Clynen et al., 2014; Dobolyi et al., 2014; Nikitidou Ledri et al.,
213 2016). These data prompted us to quantify the incidence of Dense Core Vesicles (DCV) in synaptic terminals. To this
214 aim, we performed electron microscopy on samples collected from control and experimental animals and found no
215 difference in the number of DCV across the three conditions (**Fig. 3C**). However, we found a tightening of synaptic
216 vesicle clusters at excitatory synapses in both the Acute and Chronic groups and at inhibitory terminals in the Acute
217 group (**Fig. 3D**). We limited our analysis to non-released vesicles, whose position is less likely to have been affected by
218 recent recycling. Since the increase in CPE levels did not affect DCV incidence and given the changes in synaptic
219 vesicles clustering at excitatory terminals in epileptic mice, we speculated that CPE might principally act through the
220 pathways involved in vesicles organization (Ji et al., 2017).

221

FIGURE 3

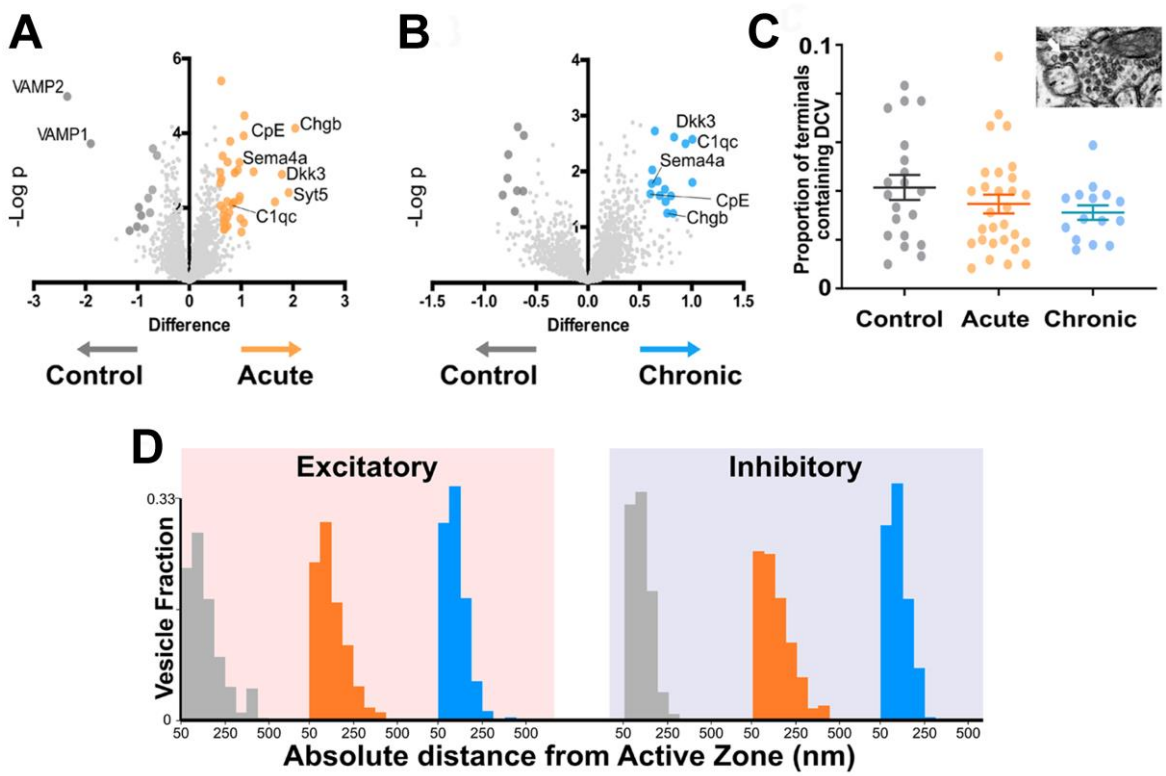

Figure 3: *Proteomics analysis of synaptosomes reveal an increase of proteins involved in vesicular positioning*. ***A, B****) Differentially expressed proteins in Control vs Acute (****A****) and Chronic epileptic phase (****B****). Volcano plots are built plotting average ratio of TeNT vs. corresponding control against their t-test log P-values; significance thresholds: FDR > 0.05 and fold change > 0.6. Proteins significantly upregulated in Acute and Chronic tetanic animals are highlighted, respectively in orange and light blue; proteins significantly downregulated are in dark grey. Proteins abbreviations are Dkk3: Dickkopf-related protein 3; Sema4a: Semaphorin 4A; Cpe: carboxypeptidase e; Chgb: chromogranin b; Syt5: synaptotagmin5; VAMP1: Vesicle-associated membrane protein 1; VAMP2: Vesicle-associated membrane protein 2; C1qc: Complement C1q C Chain.* ***C)*** *Proportion of presynaptic terminals containing Dense Core Vesicles in different non-overlapping sampled areas of Control (grey; n=20), Acute (orange; n=29) and Chronic (blue; n=15) groups. No differences between groups (One Way ANOVA, p = 0.2869). Data are represented as mean ± SEM. Inset, a representative image of Dense Core Vesicles.* ***D)*** *Right: Distribution of distances of non-released vesicles from active zone at excitatory synapses in Control (grey; n=2140), Acute (orange; n=2503) and Chronic (blue; n=5705) groups (One-way ANOVA; F=238.15, p<0.0001, Control vs Acute: p<0.0001; Control vs Chronic: p<0.0001). Left: Distribution of distances of non-released vesicles from active zone at inhibitory synapses in Chronic (grey; n=543), Acute (orange; n=717) and Chronic (blue; n=1520) groups (F=75.57, p<0.0001, Control vs Acute: p<0.0001; Control vs Chronic: p>0.05).*

222

223

224 Acute Carboxypeptidase E inhibition reduces seizure activity in epileptic mice

225 Based on the indication that CPE is upregulated in TeNT-injected mice, and given its potential involvement in
226 vesicle positioning (Ji et al., 2017), we decided to perform *in vivo* electrophysiological recordings in acute epileptic
227 mice before and after pharmacological inhibition of CPE. We performed local field potential (LFP) recordings using a
228 16-channel silicon probe, spanning the whole cortical thickness in awake epileptic mice. Recording channels were

229 divided in superficial (channels 1-5), intermediate (6-11) and deep (12-16) according to their position in the primary
230 visual cortex. After baseline recording of seizures, we topically administered on the visual cortex GEMSA, a CPE
231 inhibitor (**Fig. 4A, 4B**). The recording sessions following GEMSA administration showed a significant decrease in LFP
232 coastline (**Fig. 4C**), indicating that CPE inhibition reduces indicators of seizure activity in epileptic mice.
233

FIGURE 4

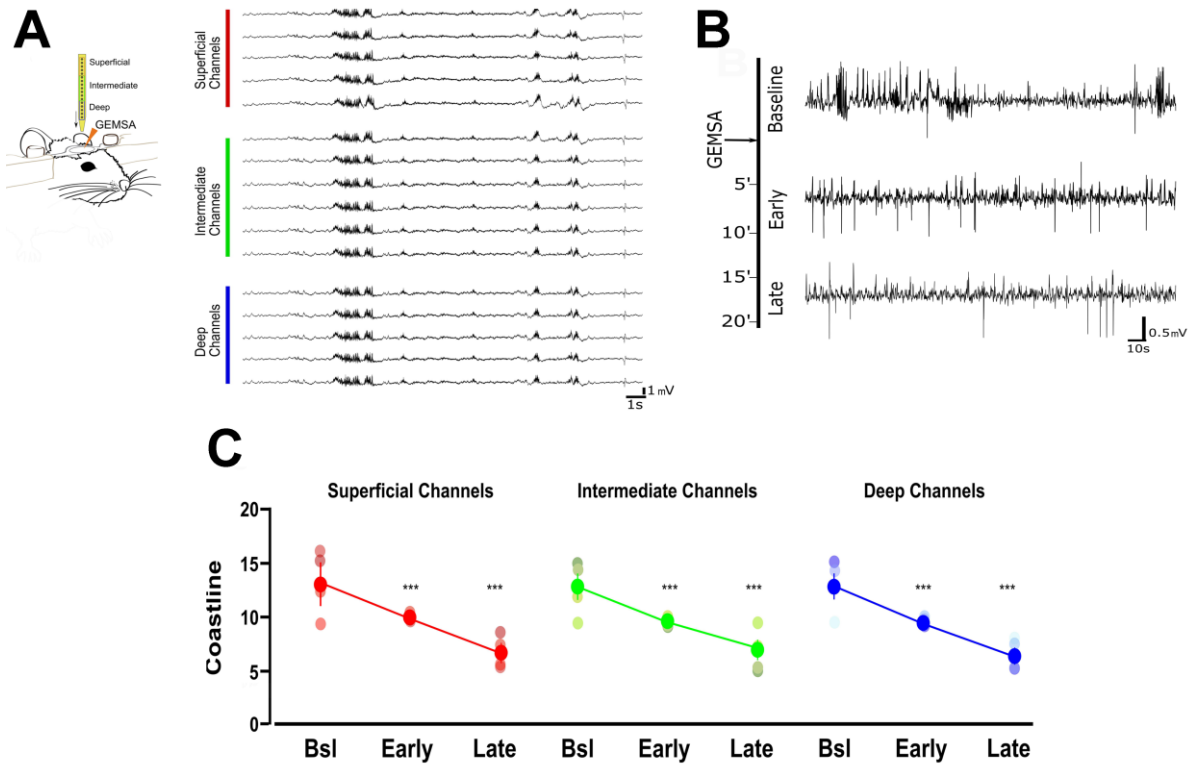

Figure 4: *Acute inhibition of Carboxypeptidase (CPE) decreases hyperexcitability in TeNT-injected mice.* ***A****) Left: diagram of experimental design: a 16-channel silicone probe was used to record LFP in different layers of the primary visual cortex, channels were analysed in 3 groups according to their recording sites in relation to the surface of the cortex: the 5 most superficial, the 5 deepest and the 6 intermediate channels. GEMSA was applied locally to inhibit CPE activity. Right: Examples of LFP traces obtained with a 16-channels probe from the visual cortex of an Acute epileptic mouse.* ***B****) LFP traces of an Acute epileptic mouse before (baseline, top) and after GEMSA administration at two different time points: early (5 to 10 minutes) and late (10 to 20 minutes).* ***C****) Coastline analysis of LFP signals recorded before (baseline) and after GEMSA administration at early and late time points. The analysis was differentially performed for superficial (left, red), intermediate (middle, green) and deep (right, blue) channels (Two-way ANOVA, Channel factor $p>0.05$, Time factor $p<0.001$; Baseline vs Early: $p < 0.01$, Baseline vs Late: $p < 0.001$, Early vs Late: $p < 0.001$, n=4). The mean, SEM and value of individual recordings are shown for each group.*

234

235 **Discussion**

236 This study provides new insights into functional and ultrastructural synaptic changes in epileptic neuronal
237 networks. Using a well-established model of epilepsy, we observed differential regulation of vesicular positioning and
238 active zone size at excitatory and inhibitory synapses (**Fig. 1, 2**). We identified a homeostatic increase in active zone
239 length specifically at inhibitory synapses, consistent with previous reports and our finding that GABA release is
240 preferentially impaired by TeNT (Schiavo et al., 2000; Ferecskó et al., 2015). These early changes at inhibitory synapses

are also consistent with previous observations made in the acute phase, when TeNT catalytic activity can still be detected (i.e. 10 days after TeNT-injection) (Mainardi et al., 2012; Vannini et al., 2016). We suggest that active zone length at inhibitory synapses is homeostatically upregulated in an attempt to restore baseline GABAergic release in spite of TeNT activity. We speculate that the lengthening of inhibitory active zones is later 'discarded', as a homeostatic mechanism, given its inability to overcome TeNT-induced reduction in vesicle release, as demonstrated by the reduced ratio of released GABAergic vesicles in both Acute and Chronic groups (**Fig. 1B**).

Ultrastructural changes of release competent vesicle positioning at excitatory synapses can only be detected at a later stage. In the chronic phase, excitatory terminals contained a smaller proportion of docked release-competent vesicles, consistent with the reported loss in spatial bias. A similar spatial reorganization of release competent vesicles can be achieved pharmacologically by stabilising actin, leading to a slower release rate during 10 Hz stimulation (Marra et al., 2012), its opposite, a tightening of synaptic vesicles, can be observed following Long-Term Potentiation in slices (Rey et al., 2020). Here, we report that spatial organization of release-competent synaptic vesicles can be modulated *in vivo*. During the chronic phase, released glutamatergic vesicles are positioned farther away from the active zone, potentially to limit their re-use during high-frequency activity. This loss of spatial bias may reduce the likelihood of generating spontaneous discharges in hyperexcitable networks. While a direct measure of the functional impact of this spatial reorganization is not possible with currently available methods, we can speculate that the reduction of released vesicles at the active zone of excitatory synapses may fit with the models of occupancy and two-step release proposed over the years by the Marty's lab (Trigo et al., 2012; Pulido et al., 2015; Pulido and Marty, 2017; Miki et al., 2018). Interpreted in the light of Marty's work, excitatory synapses in the chronic phase, although not changing in release fraction, may have a broader range of release latencies due to a reduction in occupancy at rest (Pulido et al., 2015; Pulido and Marty, 2017; Miki et al., 2018). Thus, in chronic epileptic mice the spatial organisation of release-competent vesicles farther from active zone may represent an attempt to homeostatically reduce networks' synchronicity without affecting the total number of vesicles released. While not sufficient to block seizures in TeNT epileptic model, this spatial rearrangement may account for the reported reduction of seizures observed in the chronic phase (Vallone et al., 2016; Vannini et al., 2016; Chang et al., 2018). To dissect the molecular mechanisms underlying this change in spatial bias, we performed an unbiased analysis of synaptosomes content in the two different phases of epilepsy. Unsurprisingly, we found upregulation of several proteins involved in DCV trafficking as expected during intense synaptic remodelling. However, we did not find any statistical differences in the number of DCV present in the three experimental groups. We focussed our study on CPE, a protein that is involved in many different pathways, including neuropeptides' synthesis and WNT/BDNF signalling, that was also hypothesized to regulate synaptic vesicles trafficking and positioning (Bamji et al., 2006; Staras et al., 2010; Skalka et al., 2016). Although the exact role of CPE is not completely clear, we reported a reduced hyperexcitability of acute epileptic mice after the administration of its inhibitor (**Fig. 4**). We also showed a tightening of synaptic vesicle clusters, measured from the active zone (**Fig. 3D, 3E**). Therefore our loss of spatial bias in recently released vesicles might happen on a background of overall contraction of vesicular clusters. This observation offers a possible interpretation for the effect of CPE inhibition on epileptiform activity, that was electrophysiologically measured *in vivo* (**Fig. 4**). The mechanisms by which CPE inhibition impacts on seizures remain to be fully clarified. CPE is involved in several different biosynthetic and signalling pathways (i.e. WNT, BDNF) which may account for the anti-epileptic effects. Moreover, CPE impact is likely to be indirect and very hard to dissect *in vivo*. However, further studies on other epileptic models are necessary

280 to better elucidate CPE role in epilepsy. Taken together, our results suggest a complex landscape of molecular and
281 ultrastructural changes evolving over time, opening intriguing questions regarding the temporal evolution of
282 homeostatic changes in response to the induction of hyperexcitability. It would be particularly interesting to observe
283 how homeostatic regulation of excitability adapts over development, for example in a model of genetic epilepsy,
284 where epileptogenic factors are present since the very early formation of the nervous system (Lignani et al., 2020).
285 Since TeNT-induced epilepsy is pharmacoresistant (Nilsen et al., 2005) and refractory seizures represent a major
286 unmet medical need, drugs acting on CPE levels and other regulators of synaptic pools warrant further investigation as
287 possible therapeutic treatments in currently intractable epilepsy.
288
289
290 **Acknowledgements**
291 We thank Francesca Biondi (CNR Pisa) for the excellent animal care, Natalie Allcock and Ania Straatman-Iwanowska for
292 the invaluable electron microscopy technical support and the scidraw.io team for the freely available vector graphics
293 used in Figures 1 and 4. During manuscript elaboration, EV was supported by a postdoctoral fellowship released by
294 Fondazione Umberto Veronesi (Milan, Italy). This work was funded by Epilepsy Research UK (pilot grant PGE1501 and
295 project grant P1802) and by the Wellcome Trust Seed Award in Science (108201/Z/15/Z). We also gratefully
296 acknowledge the financial support of CNR (Joint Laboratories project). This manuscript has been released as a pre-
297 print at bioRxiv (Vannini et al., 2020) https://doi.org/10.1101/2020.01.05.895029.
298
299 **Declaration of interests**
300 The authors declare no competing interests.
301
302 **Author Contributions**
303 E.V., M.C., V.M., L.MD conceived and designed the experiments; E.V., L.R., M.C. supplied the animal models; M.C.,
304 V.M. supervised the work; E.V., L.R., M.D., V.M. performed the experiments; E.V., M.D., V.M. analysed the data; E.V.,
305 V.M. wrote the paper. All authors contributed to the critical revision of the manuscript.

306 **References**

307 Bamji, S. X., Rico, B., Kimes, N., and Reichardt, L. F. (2006). BDNF mobilizes synaptic vesicles and enhances synapse
308 formation by disrupting cadherin-β-catenin interactions. *J. Cell Biol.* doi:10.1083/jcb.200601087.
309 Bernard, C. (2010). Alterations in synaptic function in epilepsy. *Epilepsia* 51, 42. doi:10.1111/j.1528-
310 1167.2010.02828.x.
311 Bromfield, E. B., and Cavazos, J. E. (2006). Basic Mechanisms Underlying Seizures and Epilepsy - An Introduction to
312 Epilepsy - NCBI Bookshelf. Available at: https://www.ncbi.nlm.nih.gov/books/NBK2510/ [Accessed March 13,
313 2020].
314 Chang, B. L., Leite, M., Snowball, A., Lieb, A., Chabrol, E., Walker, M. C., et al. (2018). Semiology, clustering, periodicity
315 and natural history of seizures in an experimental occipital cortical epilepsy model. *DMM Dis. Model. Mech.*
316 doi:10.1242/dmm.036194.
317 Clynen, E., Swijsen, A., Raijmakers, M., Hoogland, G., and Rigo, J. M. (2014). Neuropeptides as Targets for the
318 Development of Anticonvulsant Drugs. *Mol. Neurobiol.* doi:10.1007/s12035-014-8669-x.
319 Corradini, I., Donzelli, A., Antonucci, F., Welzl, H., Loos, M., Martucci, R., et al. (2014). Epileptiform activity and
320 cognitive deficits in SNAP-25(+/-) mice are normalized by antiepileptic drugs. *Cereb. Cortex* 24, 364–76.
321 doi:10.1093/cercor/bhs316.
322 Darcy, K. J., Staras, K., Collinson, L. M., and Goda, Y. (2006). Constitutive sharing of recycling synaptic vesicles between
323 presynaptic boutons. *Nat. Neurosci.* doi:10.1038/nn1640.
324 Davis, G. W., and Müller, M. (2015). Homeostatic Control of Presynaptic Neurotransmitter Release. *Annu. Rev. Physiol.*
325 doi:10.1146/annurev-physiol-021014-071740.
326 Dobolyi, A., Kekesi, K. A., Juhasz, G., Szekely, A. D., Lovas, G., and Kovacs, Z. (2014). Receptors of Peptides as
327 Therapeutic Targets in Epilepsy Research. *Curr. Med. Chem.* doi:10.2174/0929867320666131119154018.
328 Farisello, P., Boido, D., Nieus, T., Medrihan, L., Cesca, F., Valtorta, F., et al. (2013). Synaptic and extrasynaptic origin of
329 the excitation/inhibition imbalance in the hippocampus of synapsin I/II/III knockout mice. *Cereb. Cortex* 23, 581–
330 93. doi:10.1093/cercor/bhs041.
331 Ferecskó, A. S., Jiruska, P., Foss, L., Powell, A. D., Chang, W.-C., Sik, A., et al. (2015). Structural and functional
332 substrates of tetanus toxin in an animal model of temporal lobe epilepsy. *Brain Struct. Funct.* 220, 1013–1029.
333 doi:10.1007/s00429-013-0697-1.
334 Giordano, N., Iemolo, A., Mancini, M., Cacace, F., De Risi, M., Latagliata, E. C., et al. (2018). Motor learning and
335 metaplasticity in striatal neurons: Relevance for Parkinson's disease. *Brain*. doi:10.1093/brain/awx351.
336 González, O. C., Krishnan, G. P., Timofeev, I., and Bazhenov, M. (2019). Ionic and synaptic mechanisms of seizure
337 generation and epileptogenesis. *Neurobiol. Dis.* 130. doi:10.1016/j.nbd.2019.104485.
338 Harris, K. M., and Weinberg, R. J. (2012). Ultrastructure of synapses in the mammalian brain. *Cold Spring Harb.*
339 *Perspect. Biol.* doi:10.1101/cshperspect.a005587.
340 Holmes, G. L. (2015). Cognitive impairment in epilepsy: The role of network abnormalities. *Epileptic Disord.* 17, 101–
341 116. doi:10.1684/epd.2015.0739.
342 Jensen, F. E., and Harris, K. M. (1989). Preservation of neuronal ultrastructure in hippocampal slices using rapid
343 microwave-enhanced fixation. *J. Neurosci. Methods*. doi:10.1016/0165-0270(89)90146-5.

344 Ji, L., Wu, H.-T., Qin, X.-Y., and Lan, R. (2017). Dissecting carboxypeptidase E: properties, functions and
345 pathophysiological roles in disease. doi:10.1530/EC-17-0020.
346 Jiruska, P., Finnerty, G. T., Powell, A. D., Lofti, N., Cmejla, R., and Jefferys, J. G. R. (2010). Epileptic high-frequency
347 network activity in a model of non-lesional temporal lobe epilepsy. *Brain* 133, 1380–1390.
348 doi:10.1093/brain/awq070.
349 Kovac, S., and Walker, M. C. (2013). Neuropeptides in epilepsy. *Neuropeptides*. doi:10.1016/j.npep.2013.10.015.
350 Kwan, P., Schachter, S. C., and Brodie, M. J. Drug-Resistant Epilepsy.
351 Lignani, G., Baldelli, P., and Marra, V. (2020). Homeostatic Plasticity in Epilepsy. *Front. Cell. Neurosci.* 14.
352 doi:10.3389/fncel.2020.00197.
353 Lim, L., Mi, D., Llorca, A., and Marín, O. (2018). Development and Functional Diversification of Cortical Interneurons.
354 *Neuron*. doi:10.1016/j.neuron.2018.10.009.
355 Mainardi, M., Pietrasanta, M., Vannini, E., Rossetto, O., and Caleo, M. (2012). Tetanus neurotoxin-induced epilepsy in
356 mouse visual cortex. *Epilepsia* 53, 132–136. doi:10.1111/j.1528-1167.2012.03510.x.
357 Marra, V., Burden, J. J., Crawford, F., and Staras, K. (2014). Ultrastructural readout of functional synaptic vesicle pools
358 in hippocampal slices based on FM dye labeling and photoconversion. *Nat. Protoc.* 9, 1337–1347.
359 doi:10.1038/nprot.2014.088.
360 Marra, V., Burden, J. J., Thorpe, J. R., Smith, I. T., Smith, S. L., Häusser, M., et al. (2012). A Preferentially Segregated
361 Recycling Vesicle Pool of Limited Size Supports Neurotransmission in Native Central Synapses. *Neuron* 76, 579–
362 589. doi:10.1016/j.neuron.2012.08.042.
363 Meyer, H. S., Schwarz, D., Wimmer, V. C., Schmitt, A. C., Kerr, J. N. D., Sakmann, B., et al. (2011). Inhibitory
364 interneurons in a cortical column form hot zones of inhibition in layers 2 and 5A. *Proc. Natl. Acad. Sci. U. S. A.*
365 doi:10.1073/pnas.1113648108.
366 Miki, T., Nakamura, Y., Malagon, G., Neher, E., and Marty, A. (2018). Two-component latency distributions indicate
367 two-step vesicular release at simple glutamatergic synapses. *Nat. Commun.* doi:10.1038/s41467-018-06336-5.
368 Nikitidou Ledri, L., Melin, E., Christiansen, S. H., Gøtzsche, C. R., Cifra, A., Woldbye, D. P. D., et al. (2016). Translational
369 approach for gene therapy in epilepsy: Model system and unilateral overexpression of neuropeptide Y and Y2
370 receptors. *Neurobiol. Dis.* 86, 52–61. doi:10.1016/j.nbd.2015.11.014.
371 Nilsen, K. E., Walker, M. C., and Cock, H. R. (2005). Characterization of the tetanus toxin model of refractory focal
372 neocortical epilepsy in the rat. *Epilepsia*. doi:10.1111/j.0013-9580.2005.26004.x.
373 Pellegrini, D., Del Grosso, A., Angella, L., Giordano, N., Dilillo, M., Tonazzini, I., et al. (2019). Quantitative
374 microproteomics based characterization of the central and peripheral nervous system of a mouse model of
375 Krabbe disease. *Mol. Cell. Proteomics*. doi:10.1074/mcp.RA118.001267.
376 Pitkänen, A., and Immonen, R. (2014). Epilepsy Related to Traumatic Brain Injury. *Neurotherapeutics* 11, 286–296.
377 doi:10.1007/s13311-014-0260-7.
378 Pitkänen, A., Lukasiuk, K., Edward Dudek, F., and Staley, K. J. (2015). Epileptogenesis. *Cold Spring Harb. Perspect. Med.*
379 5. doi:10.1101/cshperspect.a022822.
380 Pitkänen, A., Nehlig, A., Brooks-Kayal, A. R., Dudek, F. E., Friedman, D., Galanopoulou, A. S., et al. (2013). Issues related
381 to development of antiepileptogenic therapies. *Epilepsia* 54, 35–43. doi:10.1111/epi.12297.
382 Plubell, D. L., Wilmarth, P. A., Zhao, Y., Fenton, A. M., Minnier, J., Reddy, A. P., et al. (2017). Extended multiplexing of

383 tandem mass tags (TMT) labeling reveals age and high fat diet specific proteome changes in mouse epididymal
384 adipose tissue. *Mol. Cell. Proteomics*. doi:10.1074/mcp.M116.065524.
385 Pulido, C., and Marty, A. (2017). Quantal fluctuations in central mammalian synapses: Functional role of vesicular
386 docking sites. *Physiol. Rev.* doi:10.1152/physrev.00032.2016.
387 Pulido, C., Trigo, F. F., Llano, I., and Marty, A. (2015). Vesicular Release Statistics and Unitary Postsynaptic Current at
388 Single GABAergic Synapses. *Neuron*. doi:10.1016/j.neuron.2014.12.006.
389 Rey, S., Marra, V., Smith, C., and Staras Correspondence, K. (2020). Nanoscale Remodeling of Functional Synaptic
390 Vesicle Pools in Hebbian Plasticity. *CellReports* 30, 2006-2017.e3. doi:10.1016/j.celrep.2020.01.051.
391 Rossi, L. F., Wykes, R. C., Kullmann, D. M., and Carandini, M. (2017). Focal cortical seizures start as standing waves and
392 propagate respecting homotopic connectivity. *Nat. Commun.* 8, 1–11. doi:10.1038/s41467-017-00159-6.
393 Rubin, R., Abbott, L. F., and Sompolinsky, H. (2017). Balanced excitation and inhibition are required for high-capacity,
394 noise-robust neuronal selectivity. *Proc. Natl. Acad. Sci. U. S. A.* 114, E9366–E9375.
395 doi:10.1073/pnas.1705841114.
396 Schiavo, G., Matteoli, M., and Montecucco, C. (2000). Neurotoxins affecting neuroexocytosis. *Physiol. Rev.*
397 doi:10.1152/physrev.2000.80.2.717.
398 Sharma, A. K., Rani, E., Waheed, A., and Rajput, S. K. (2015). Pharmacoresistant Epilepsy: A Current Update on Non-
399 Conventional Pharmacological and Non-Pharmacological Interventions. *J. Epilepsy Res.* 5, 1–8.
400 doi:10.14581/jer.15001.
401 Skalka, N., Caspi, M., Lahav-Ariel, L., Loh, Y. P., Hirschberg, K., and Rosin-Arbesfeld, R. (2016). Carboxypeptidase E
402 (CPE) inhibits the secretion and activity of Wnt3a. *Oncogene* 35, 6416–6428. doi:10.1038/onc.2016.173.
403 Snowball, A., Chabrol, E., Wykes, R. C., Shekh-Ahmad, T., Cornford, J. H., Lieb, A., et al. (2019). Epilepsy gene therapy
404 using an engineered potassium channel. *J. Neurosci.* doi:10.1523/JNEUROSCI.1143-18.2019.
405 Sohal, V. S., and Rubenstein, J. L. R. (2019). Excitation-inhibition balance as a framework for investigating mechanisms
406 in neuropsychiatric disorders. *Mol. Psychiatry* 24, 1248–1257. doi:10.1038/s41380-019-0426-0.
407 Spalletti, C., Alia, C., Lai, S., Panarese, A., Conti, S., Micera, S., et al. (2017). Combining robotic training and inactivation
408 of the healthy hemisphere restores pre-stroke motor patterns in mice. *Elife*. doi:10.7554/eLife.28662.
409 Staras, K., Branco, T., Burden, J. J., Pozo, K., Darcy, K., Marra, V., et al. (2010). A Vesicle Superpool Spans Multiple
410 Presynaptic Terminals in Hippocampal Neurons. *Neuron* 66, 37–44. doi:10.1016/j.neuron.2010.03.020.
411 Tremblay, R., Lee, S., and Rudy, B. (2016). GABAergic Interneurons in the Neocortex: From Cellular Properties to
412 Circuits. *Neuron*. doi:10.1016/j.neuron.2016.06.033.
413 Trigo, F. F., Sakaba, T., Ogden, D., and Marty, A. (2012). Readily releasable pool of synaptic vesicles measured at single
414 synaptic contacts. *Proc. Natl. Acad. Sci. U. S. A.* doi:10.1073/pnas.1209798109.
415 Turrigiano, G. (2012). Homeostatic synaptic plasticity: Local and global mechanisms for stabilizing neuronal function.
416 *Cold Spring Harb. Perspect. Biol.* doi:10.1101/cshperspect.a005736.
417 Turrigiano, G. G. (2008). The Self-Tuning Neuron: Synaptic Scaling of Excitatory Synapses. *Cell*.
418 doi:10.1016/j.cell.2008.10.008.
419 Vallone, F., Vannini, E., Cintio, A., Caleo, M., and Di Garbo, A. (2016). Time evolution of interhemispheric coupling in a
420 model of focal neocortical epilepsy in mice. *Phys. Rev. E* 94, 032409. doi:10.1103/PhysRevE.94.032409.
421 van Versendaal, D., and Levelt, C. N. (2016). Inhibitory interneurons in visual cortical plasticity. *Cell. Mol. Life Sci.*

422 doi:10.1007/s00018-016-2264-4.
423 Vannini, E., Caleo, M., Chillemi, S., and Di Garbo, A. (2017). Dynamical properties of LFPs from mice with unilateral
424 injection of TeNT. *BioSystems* 161, 57–66. doi:10.1016/j.biosystems.2017.09.009.
425 Vannini, E., Restani, L., Dilillo, M., McDonnell, L., Caleo, M., and Marra, V. (2020). Focal epilepsy modulates vesicular
426 positioning at cortical synapses. *bioRxiv*, 2020.01.05.895029. doi:10.1101/2020.01.05.895029.
427 Vannini, E., Restani, L., Pietrasanta, M., Panarese, A., Mazzoni, A., Rossetto, O., et al. (2016). Altered sensory
428 processing and dendritic remodeling in hyperexcitable visual cortical networks. *Brain Struct. Funct.* 221, 2919–
429 2936. doi:10.1007/s00429-015-1080-1.
430 Vezzani, A., and Sperk, G. (2004). Overexpression of NPY and Y2 receptors in epileptic brain tissue: An endogenous
431 neuroprotective mechanism in temporal lobe epilepsy? *Neuropeptides*. doi:10.1016/j.npep.2004.05.004.
432 Wasilewski, A., Serventi, J., Ibegbu, C., Wychowski, T., Burke, J., and Mohile, N. (2020). Epilepsy education in gliomas:
433 engaging patients and caregivers to improve care. *Support. Care Cancer* 28, 1405–1409. doi:10.1007/s00520-
434 019-04968-x.
435 Wefelmeyer, W., Puhl, C. J., and Burrone, J. (2016). Homeostatic Plasticity of Subcellular Neuronal Structures: From
436 Inputs to Outputs. *Trends Neurosci.* doi:10.1016/j.tins.2016.08.004.
437 Wie Børsheim, A., Engeland, A., and Gilhus, N. E. (2020). Epilepsy and autoimmune diseases: Comorbidity in a national
438 patient cohort. *Seizure* 75, 89–95. doi:10.1016/j.seizure.2019.12.015.
439 Wykes, R. C., Heeroma, J. H., Mantoan, L., Zheng, K., MacDonald, D. C., Deisseroth, K., et al. (2012). Optogenetic and
440 Potassium Channel Gene Therapy in a Rodent Model of Focal Neocortical Epilepsy. *Sci. Transl. Med.* 4, 161ra152-
441 161ra152. doi:10.1126/scitranslmed.3004190.
442 Xue, M., Atallah, B. V., and Scanziani, M. (2014). Equalizing excitation-inhibition ratios across visual cortical neurons.
443 *Nature* 511, 596–600. doi:10.1038/nature13321.
444